Chapter 2
Concrete and Reinforced Concrete Behaviour

Abstract. This chapter describes briefly the most important mechanical properties of concrete, reinforcement and reinforced concrete elements in a static and dynamic regime. In addition, bond-slip between reinforcement and concrete is discussed. Attention is laid on a size effect in concrete and reinforced concrete elements.

Concrete is still the most widely used construction material in terms of volume since it has the lowest ratio between cost and strength as compared to other available materials. It is a composite phase-material consisting mainly of aggregate, cement matrix and voids containing water or air (Fig. 2.1a). As a consequence, the concrete structure is strongly heterogeneous (Fig. 2.1b). Concrete properties depend strongly on the cement and aggregate quality and the ratio between cement and water. Classical concretes are divided into 3 groups depending upon the volumetric weight γ: heavy concretes γ=28-50 kN/m^3, normal concretes γ=20-28 kN/m^3 and light concretes γ=12-20 kN/m^3. Plain concrete is a brittle or quasi-brittle material, i.e. its bearing capacity strongly and rapidly falls down during compression and tension, and localized zones and macro-cracks are created. Its behaviour is mainly non-linear (a linear behaviour is limited to a very small range of deformation). Concrete has two undesirable properties, namely: low tensile strength and large brittleness (low energy absorption capacity) that cause collapse to occur shortly after the formation of the first crack. Therefore, the application of concrete subjected to impact, earth-quaking and fatigue loading is strongly limited. To improve these two negative properties, reinforcement in the form of bars and stirrups is mainly used.

Uniaxial Compression of Concrete

Typical curves for concrete during uniaxial compression are shown in Fig. 2.2. The material elastically behaves up to 30% of its compressive strength. Above this point, the behaviour starts to be non-linear. In the vicinity of the peak on the stress-strain curve, damage begins and the curve falls down until complete failure is reached. The cracks are parallel to the loading direction. During compression, first the volume decreases linearly then non-linearly reaching its minimum at the point M of Fig. 2.2. Next, the material is subjected to dilatancy due to formation and propagation of cracks. The Poisson's ratio remains constant (0.15-0.22) up to $0.8f_c$ (f_c – uniaxial compressive strength). At failure, it may even exceed 0.5 (Fig. 2.3). The compressive

J. Tejchman, J. Bobiński: Continuous & Discontinuous Modelling of Fracture, SSGG, pp. 5–47.
springerlink.com

strength depends on the specimen size and shape (Fig. 2.4). It decreases with increasing slenderness ratio *h/b* (or *h/d*) (*h* – specimen height, *b* – specimen width, *d* – specimen diameter). It is larger for plates than for prisms and cylinders.

The higher is the compressive strength of concrete, the larger is the material brittleness (ratio between the energy consumed after and before the stress-strain peak) (Fig. 2.5).

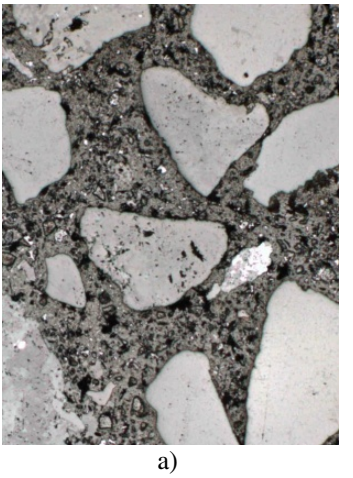

a)

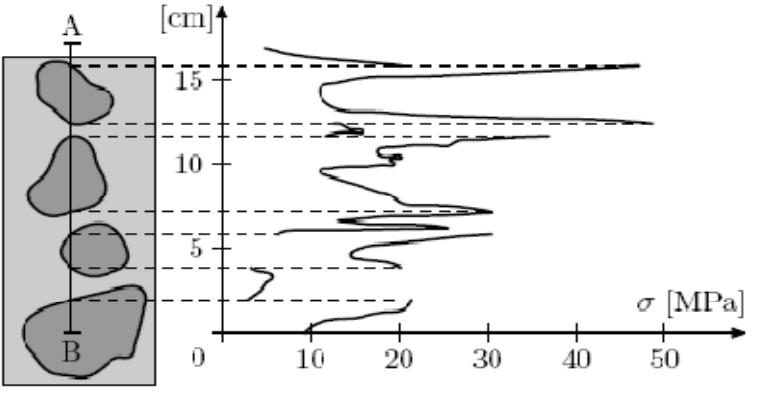

b)

Fig. 2.1 Concrete: a) non-uniform phase-structure, b) stress distribution in concrete subjected to compression by Dantu (1958) (Godycki-Ćwirko 1982, Klisiński and Mróz 1988)

Uniaxial Tension of Concrete

A typical stress-displacement diagram is shown in Fig. 2.6. The tensile strength of concrete is about 10 times lower that its compressive strength. A linear behaviour of concrete takes place up to 60% of the tensile strength f_t. A micro-crack is perpendicular to the loading direction. The material undergoes dilatancy only.

Influence of Strain Rate on Concrete

The concrete strength increases when strain rate increases due to confinement by inertial lateral restraint, shorter time for cracks to be created and viscosity of free water (Rossi 1991, Zheng and Li 2004) (Figs. 2.7 and 2.8). The material brittleness decreases with increasing strain rate. During impact loading, the compressive strength also increases; however, the material behaviour after the peak can be very different (Figs. 2.9 and 2.10). The strength of concrete after drying is not sensitive to loading rate.

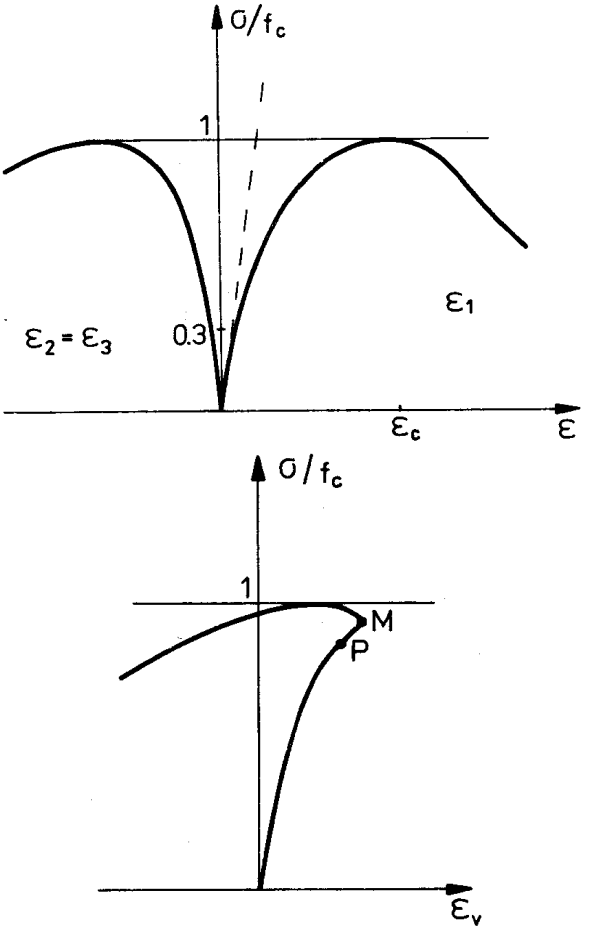

Fig. 2.2 Typical stress-strain diagram and volume changes during uniaxial vertical compression for concrete (σ - compressive normal stress, ε_1 – vertical normal strain, $\varepsilon_{2,3}$ – horizontal normal strains, ε_v – volumetric strain, f_c – uniaxial compressive strength) (Klisiński and Mróz 1988)

Biaxial Tests of Concrete

The stress-strain curves are shown in Fig. 2.11 and limit curves are depicted in Fig. 2.12. In addition, Fig. 2.13 presents volume changes. The largest increase of compressive strength during biaxial compression (by about 25%) is achieved for the ratio of the principal stresses equal to 0.6. If this ratio is equal to 1, the strength increase is about 16%.

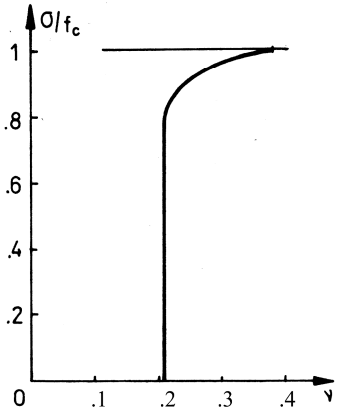

Fig. 2.3 Typical change of Poisson's ratio ν with normalized compressive stress σ/f_c during uniaxial compression (Klisiński and Mróz 1988)

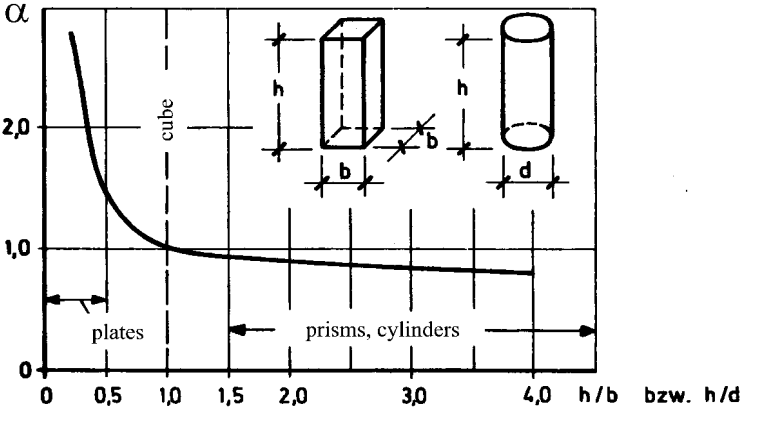

Fig. 2.4 Relationship between compressive strength of concrete prisms and compressive strength of concrete cubes α against slenderness ratio of concrete specimen *h/d* or *h/b* (Leonhard 1973)

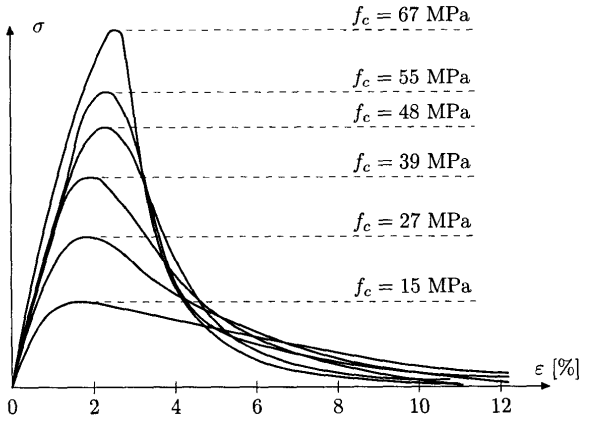

Fig. 2.5 Effect of uniaxial compression strength f_c on stress-strain relationship σ-ε (Klisiński and Mróz 1988)

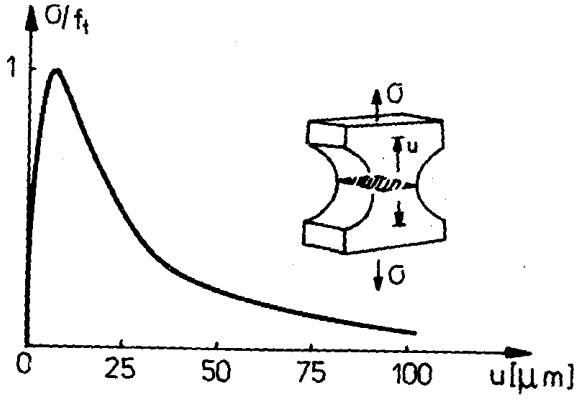

Fig. 2.6 Typical normalized stress-displacement curve during uniaxial extension for concrete (σ - vertical normal stress, u – vertical crack displacement, f_t - uniaxial tensile strength) (Klisiński and Mróz 1988)

Triaxial Tests of Concrete

Figure 2.14 demonstrates the results of monotonic usual triaxial experiments with concrete. The cylindrical specimens were initially loaded under hydrostatic confining pressure till the required value was reached. After that, horizontal confining pressure was kept constant and the specimen was subjected to increasing (Fig. 2.14) or decreasing vertical loading (Fig. 2.15). Concrete strength evidently increases with increasing confining pressure. Fig. 2.16 shows the material behaviour during hydrostatic loading, where fast material hardening is

noticeable. Fig. 2.17 shows a limit curve in plane of the octahedral and hydrostatic stress for different confining pressures, which is parabolic. In turn, Fig. 2.18 depicts the results of cyclic true triaxial tests with rectangular prismatic specimens loaded in three orthogonal directions performed by Scavuzzo et al. (1983).

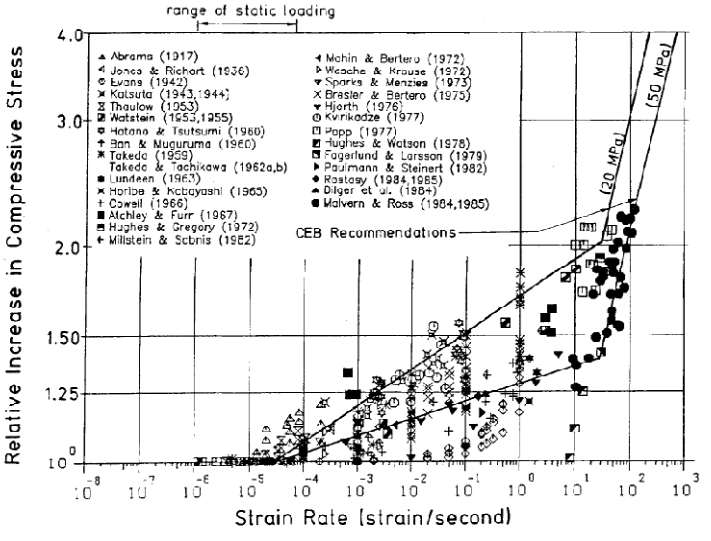

a)

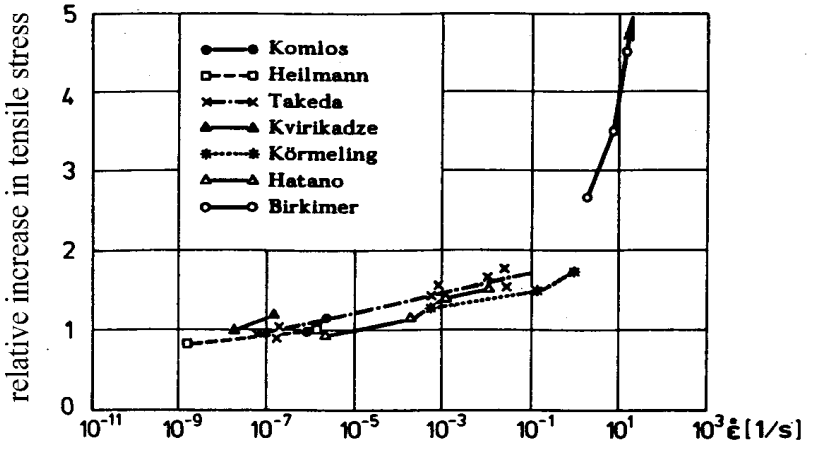

b)

Fig. 2.7 Log-log scale of relative compressive strength increase versus strain rate (a) and relative tensile strength increase versus strain rate (b) (Bischoff and Perry 1991)

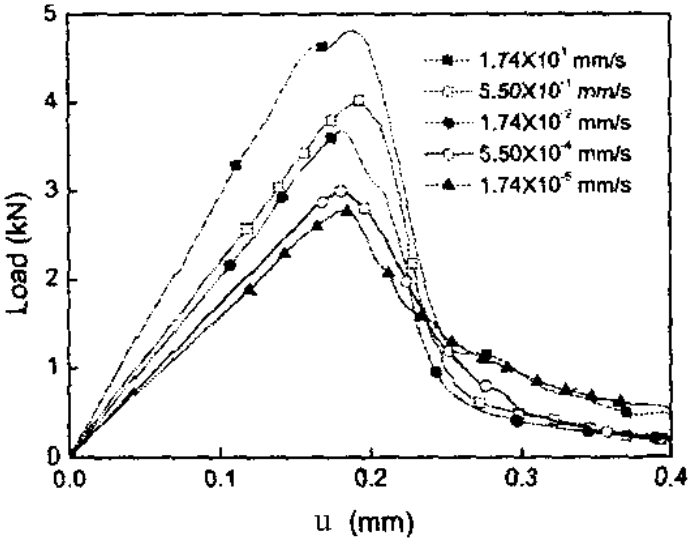

Fig. 2.8 Effect of loading velocity on concrete behaviour: load-displacement diagram during three-point bending (Zhang et al. 2009).

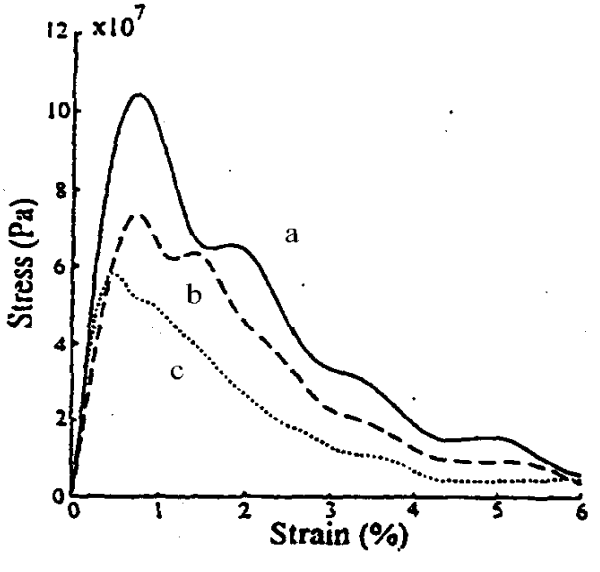

Fig. 2.9 Effect of strain rate on evolution of compressive normal stress versus normal strain: a) $d\varepsilon/dt$=700 s^{-1}, b) $d\varepsilon/dt$=500 s^{-1}, c) $d\varepsilon/dt$=300 s^{-1} (Gary 1990).

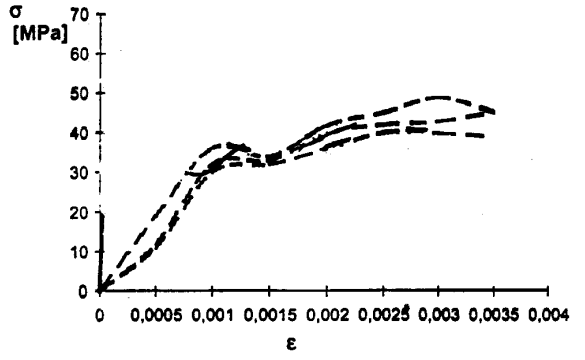

a)

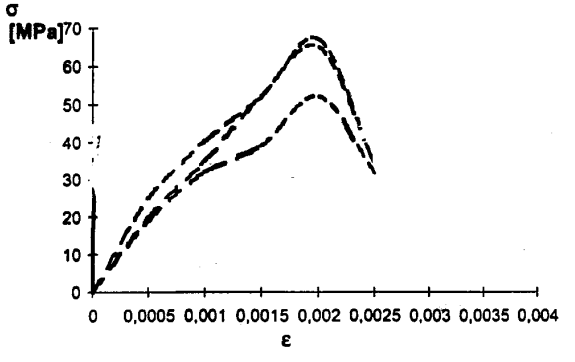

b)

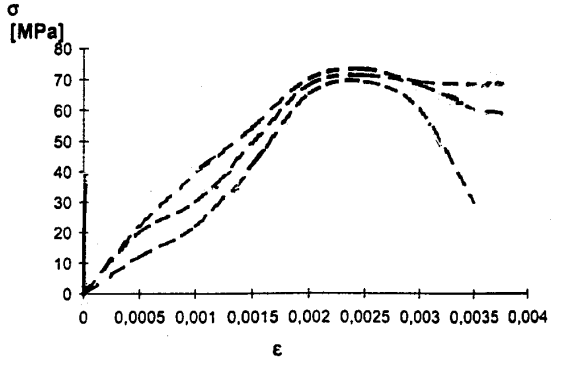

c)

Fig. 2.10 Effect of loading velocity on stress-strain curve during impact loading (a-c): a) concrete 30 MPa, impactor mass 31.6 kg, impactor velocity 8.2 m/s, $d\varepsilon/dt$=9.0 1/s, b) concrete 50 MPa, impactor mass 31.6 kg, impactor velocity 5.3 m/s, $d\varepsilon/dt$=5.2 1/s, c) concrete 50 MPa, impactor mass 78.3 kg, impactor velocity 5.3 m/s, $d\varepsilon/dt$=5.6 1/s (Bischoff and Perry 1995)

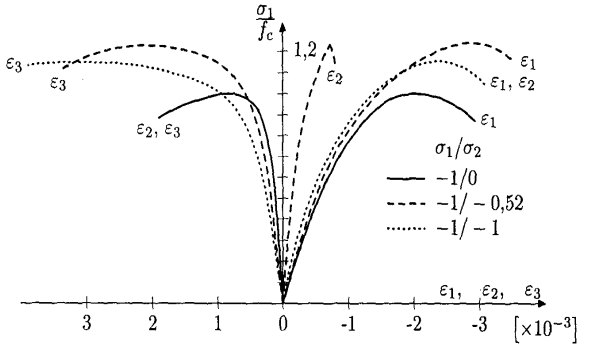

a)

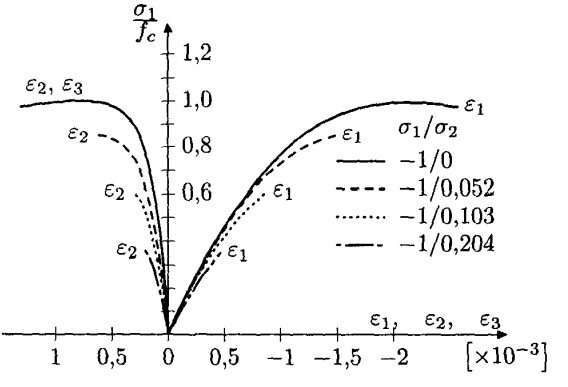

b)

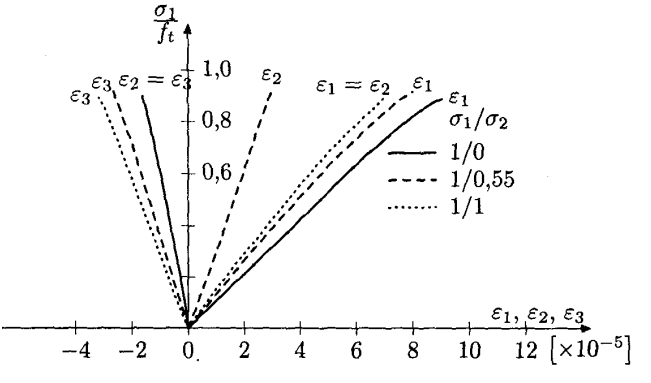

c)

Fig. 2.11 Stress-strain curves from experiments by Kupfer et al. (1969): a) biaxial compression, b) axial compression and axial tension, c) biaxial extension (Klisiński and Mróz 1988)

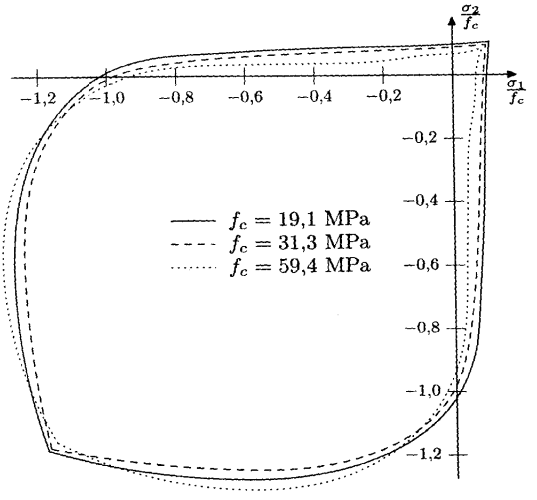

Fig. 2.12 Maximum stresses in plane stress state in biaxial tests by Kupfer et al. (1969) (Klisiński and Mróz 1988)

An approximate shape of a failure surface for concrete in the space of principal stresses based on experiments is shown in Fig. 2.19. The failure surface of concrete is symmetric against the hydrostatic line $\sigma_1=\sigma_2=\sigma_3$. The shape of the surface in a principal stress space is paraboloidal (Figs. 2.17 and 2.19). In deviatoric planes, the surface shape is approximately circular (during compression) and approximately elliptic (during tension); thus it changes from a curvilinear triangle with smoothly rounded corners to nearly circular with increasing pressure.

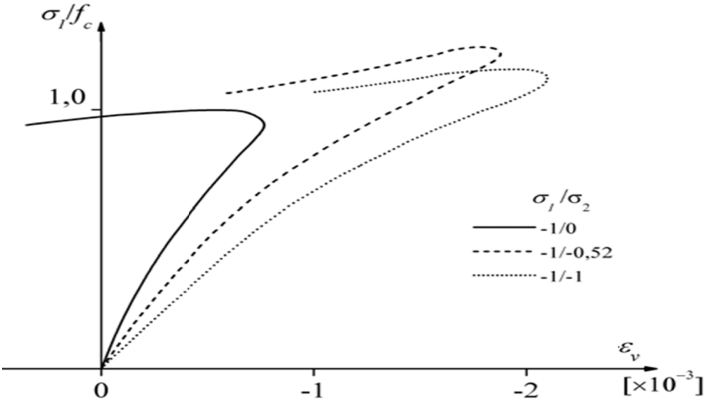

Fig. 2.13 Volume changes during biaxial tests by Kupfer et al. (1969) (Klisiński and Mróz 1988)

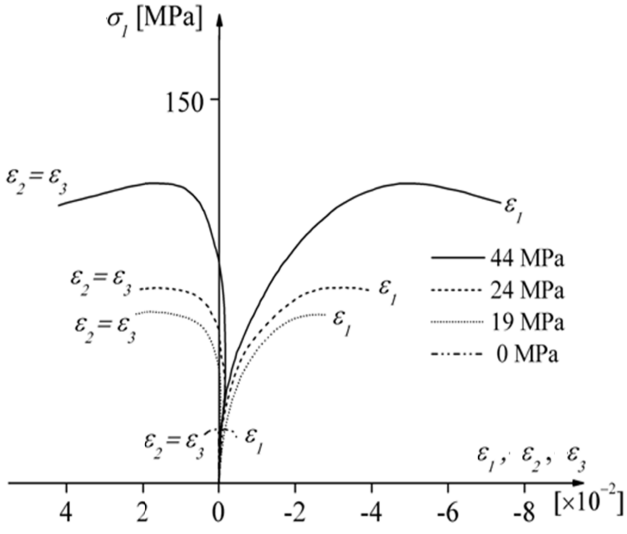

Fig. 2.14 Stress-strain curve during usual triaxial compression for different confining pressures and increasing vertical load by Kostovos and Newman (1978) and Kostovos (1980)

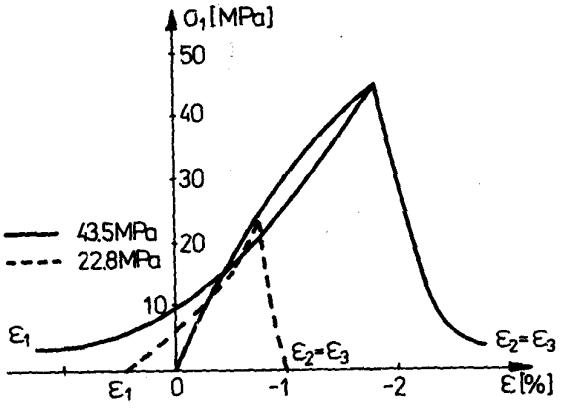

Fig. 2.15 Stress-strain curve during usual triaxial compression for different confining pressures and decreasing vertical load by Kostovos and Newman (1978) and Kotsovos (1980)

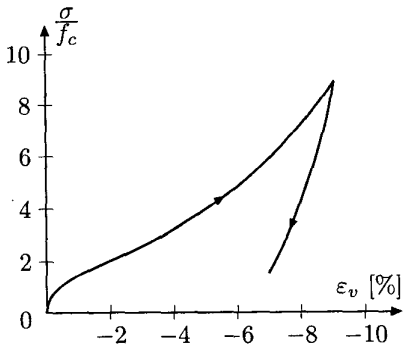

Fig. 2.16 Stress-volume strain during hydrostatic compression (Klisiński and Mróz 1998)

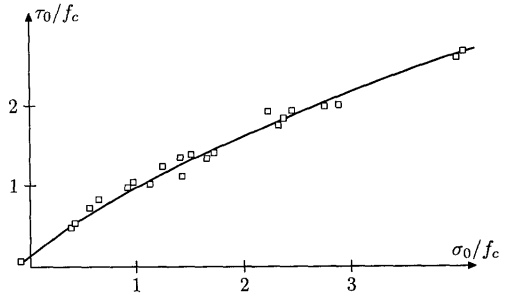

Fig. 2.17 Failure surface in plane τ_o-σ_o from usual triaxial experiments by Kotsovos (1980) (τ_o - octahedral stress, σ_o – hydrostatic stress, f_c - compressive strength) (Klisiński and Mróz 1988)

Cyclic Behaviour of Concrete

During quasi-static cyclic loading, concrete shows pronounced stiffness degradation due to fracture during both compression, tension and bending (Fig. 2.20). A hysteresis loop occurs during each cycle whose shape depends upon loading type.

Reinforcement of Concrete

The reinforcement co-operates with concrete during loading by carrying principal tensile and compressive stresses. A stress-strain diagram for different classes of reinforcement steel during uniaxial tension is shown in Fig. 2.21. A plastic region decreases with increasing tensile strength. During cyclic loading, compressive strength slightly decreases and tensile strength slightly increases (the so-called Bauschinger's effect) (Fig. 2.22).

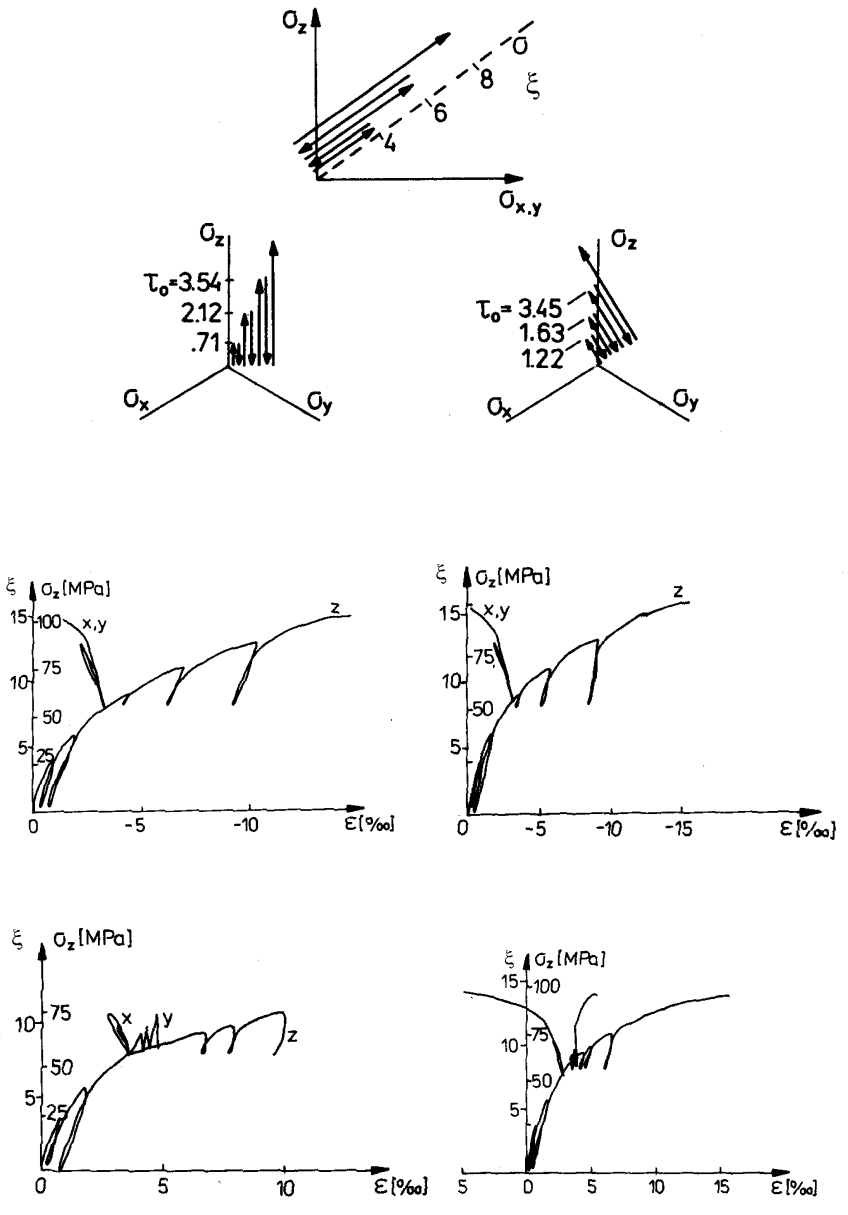

Fig. 2.18 Experimental results of cyclic true triaxial tests by Scavuzzo et al. (1983) for different stress paths (Klisiński and Mróz 1988)

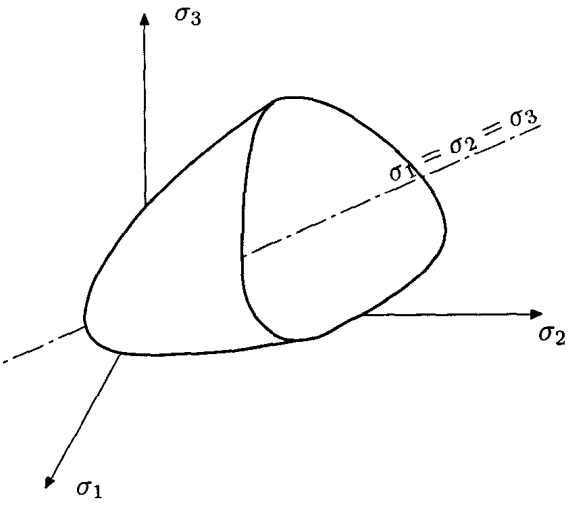

a)

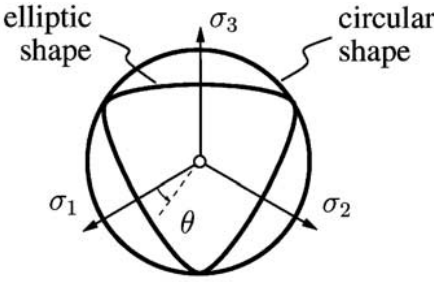

b)

Fig. 2.19 Failure surface for concrete in space of principal stresses σ_i (a) and in deviatoric plane (θ - Lode angle) (Klisiński and Mróz 1988, Pivonka et al. 2003)

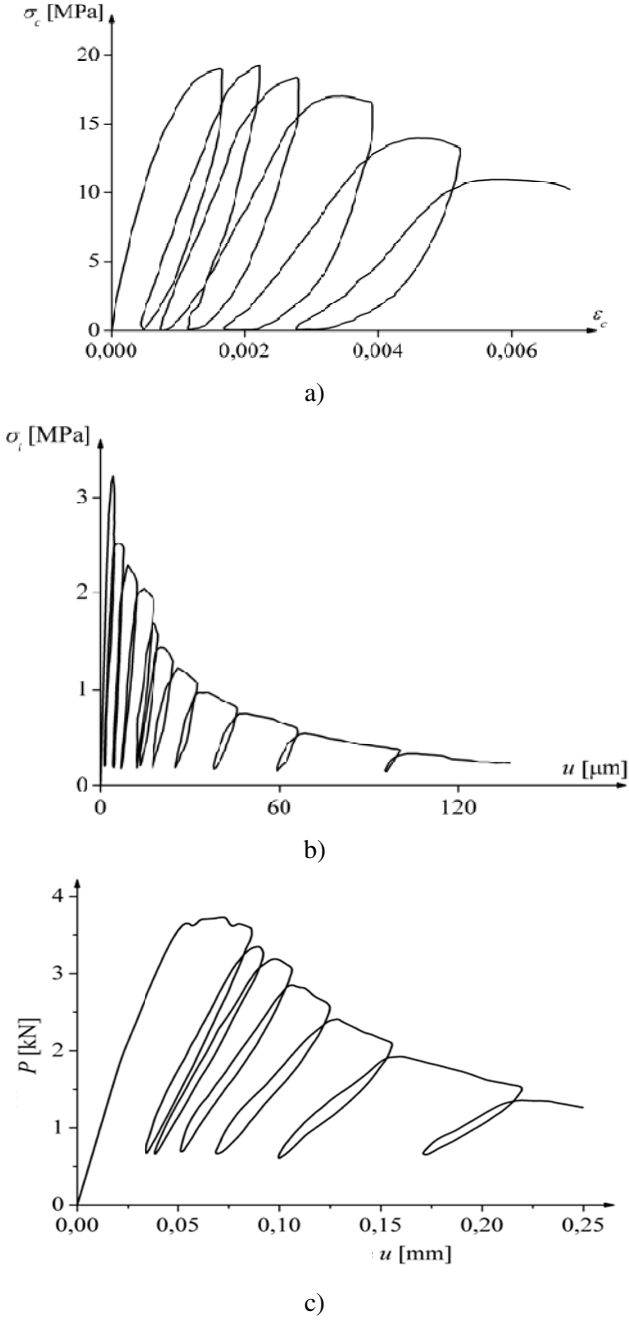

Fig. 2.20 Concrete behaviour under cyclic loading: a) stress-strain curve under uniaxial compression (Karsan and Jirsa 1969), b) stress-displacement curve under uniaxial tension (Reinhardt et al. 1986), c) force-deflection curve under four-point bending (Hordijk1991)

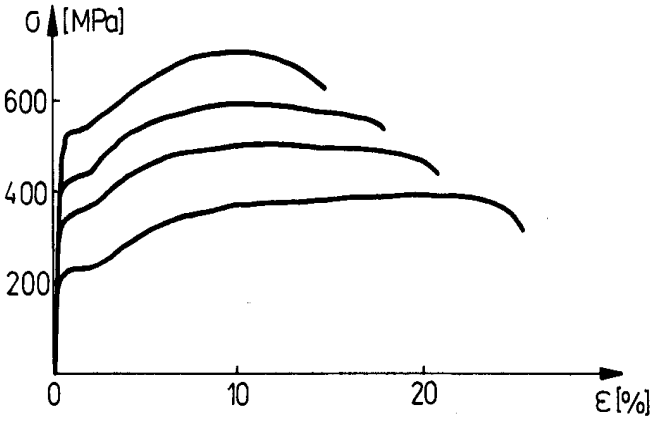

Fig. 2.21 Stress-strain diagram for reinforcement steel during uniaxial tension (Klisiński and Mróz 1988)

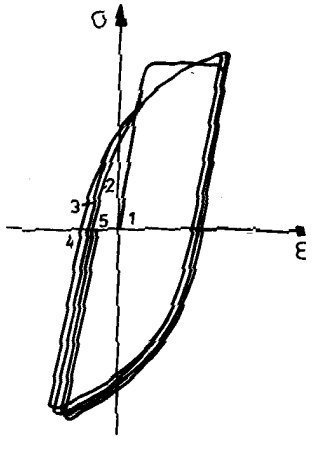

Fig. 2.22 Stress-strain diagram for reinforcement steel during cyclic loading (Klisiński and Mróz 1988)

Size Effect in Concrete Elements

Comprehensive investigations of the effect of the element size and boundary conditions along lateral surfaces during uniaxial compression were performed by van Vliet and van Mier (1995, 1996) (Fig. 2.23-2.28). The experimental results show that the both strength and ductility considerably increase with decreasing element size when large friction exists along horizontal lateral surfaces. If friction is small, the strength increase is non-significant. Fracture pattern strongly depends on boundary conditions. For large friction, cracks occur at horizontal edges only

(the mid-region remains uncracked). In the case of small friction, a macro-crack is created in the form of shear zones whose number increases with a reduction of the element size.

A pronounced size effect was observed during multi-axial compression in hollow-cylinder tests using different pressures (Elkadi and van Mier 2006) (Fig. 2.29). The compressive strength reduced with increasing element size.

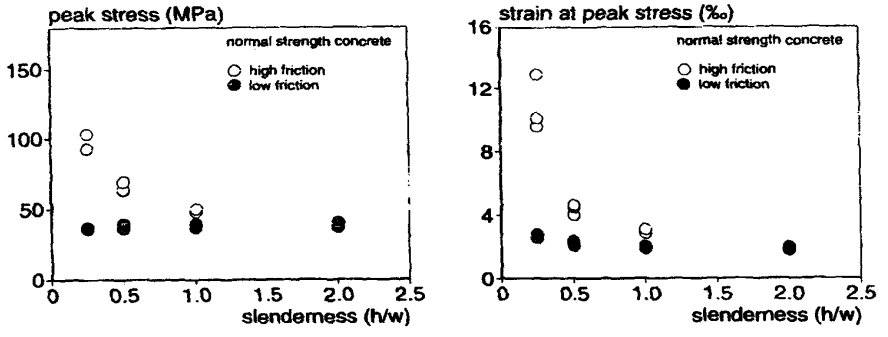

Fig. 2.23 Peak stresses and corresponding strains of the normal strength concrete during uniaxial compression specimens depending upon friction along horizontal edges (van Vliet and van Mier 1996)

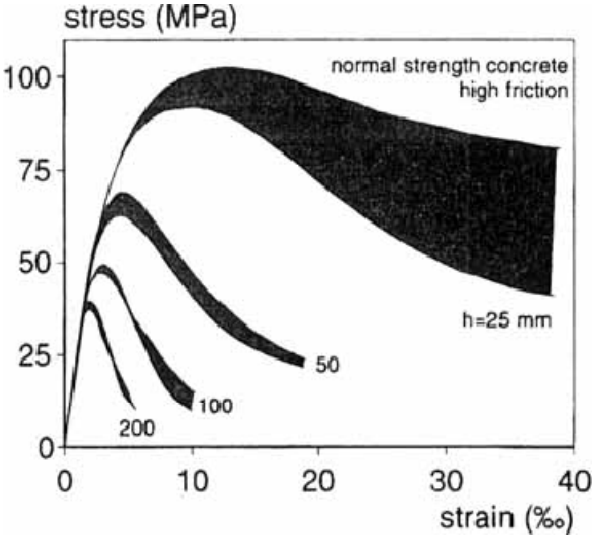

Fig. 2.24 Compressive stress-strain curves of the normal strength concrete specimens with different heights *h* and high friction boundary conditions along horizontal edges (van Vliet and van Mier 1996)

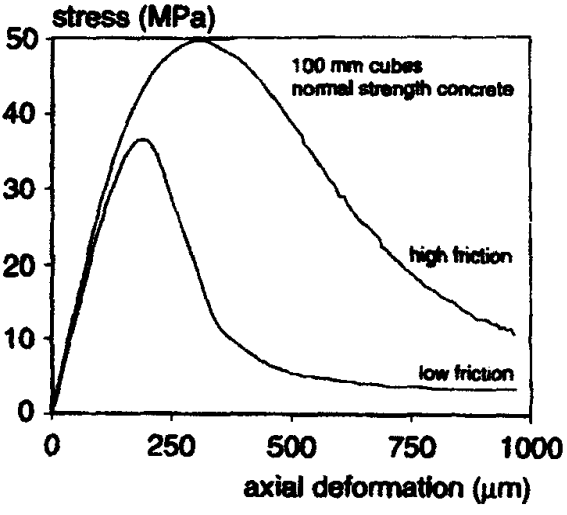

Fig. 2.25 Compressive curves for 100 mm cube specimens (normal strength concrete) loaded under high and low friction boundary conditions along horizontal edges (van Vliet and van Mier 1996)

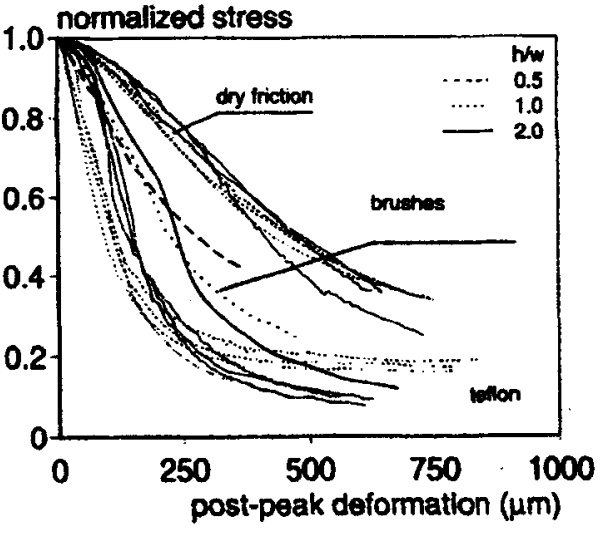

Fig. 2.26 Post-peak deformations of normal strength concrete specimens with different boundary conditions along horizontal edges (van Vliet and van Mier 1996)

A strong deterministic size effect occurred in concrete during uniaxial extension (van Vliet and van Mier 2000) (Figs. 2.30-2.32) and three-point bending (Le Bellego et al. 2003) (Figs. 2.33-2.35). In addition, a strong stochastic size

effect was observed in experiments with concrete beams of the same height and different span at the same load (Koide et al. 1998, 2000) (Fig. 2.36), i.e. the maximum bending moment clearly decreased with increasing bending span.

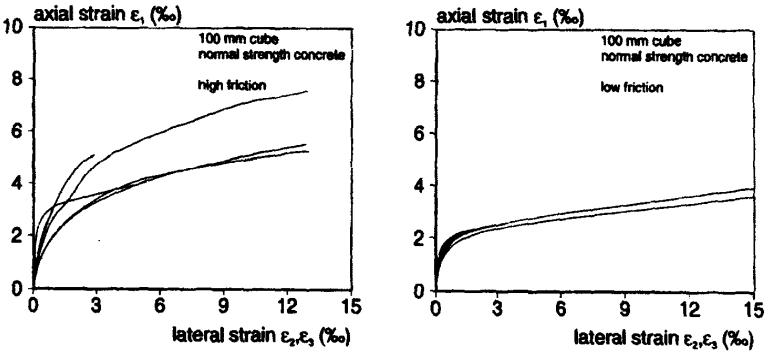

a) b)

Fig. 2.27 Axial strain against lateral strain for normal strength concrete cubes with: a) high friction and b) low friction along horizontal edges (van Vliet and van Mier 1996)

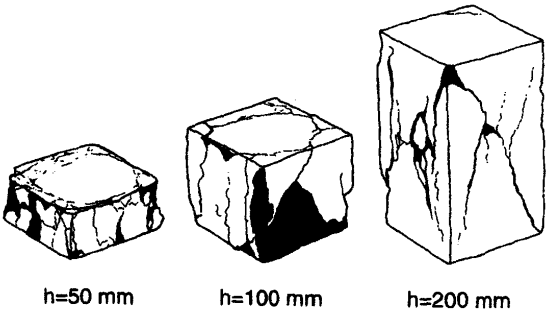

(a)

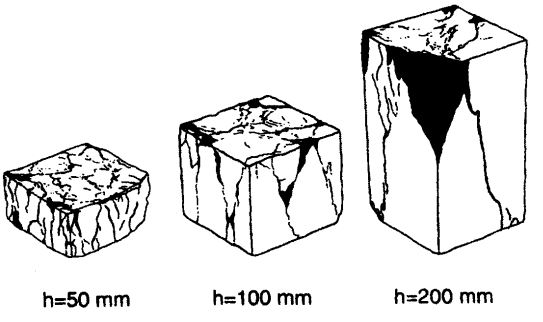

(b)

Fig. 2.28 Crack patterns of normal strength concrete specimens with high (A) and low (B) friction boundary conditions for different specimen heights *h* (van Vliet and van Mier 1996)

Size Effect in Reinforced Concrete Elements

A size effect occurs also in reinforced concrete elements when the failure by yielding of longitudinal steel bars is excluded in advance (brittle failure takes then place in a compressive concrete zone).

Figure 2.37 shows a size effect in reinforced concrete beams of the same slenderness without shear reinforcement in experiments by Leonhardt and Walther (1962). The size of beams was in a proportion 1:2:3:4. The reinforcement included always 2 steel bars. The reinforcement ratio was 1.35%. The bearing capacity of beams decreased with increasing beam size.

Comprehensive investigations on a size effect were carried out by Walraven and Lehwalter (1994) for different reinforced concrete beams. First, slender reinforced concrete beams loaded in shear without stirrups were investigated (Fig. 2.38). The beams were made of normal gravel concrete and lightweight concrete. The experiments were carried out with 3 different beams with the same thickness of b=200 mm: h=150 mm, l=2300 mm (small size beam '1'), h=450 mm, l=4100 mm (medium size beam '2') and h=750 mm, l=6400 mm (large size beam '3'). The reinforcement ratio was 0.79-0.83%: $1\times\phi_s8$ and $2\times\phi_s10$ (beam '1'), $1\times\phi_s20$ and $2\times\phi_s14$ (beam '2') and $3\times\phi_s22$ (beam '3').

Second, short reinforced concrete beams loaded in shear without and with shear reinforcement were investigated (Fig. 2.39). The beam length L varied between 680 mm and 2250 mm and the height h was between 200 mm and 1000 mm (the beam width b was always 250 mm). In the tests, the span-to-depth ratio was always 1. The reinforcement ratio of the specimens was 1.1% (the failure by yielding of longitudinal steel bars was again excluded in advance). The shear reinforcement ratio was 0%, 0.15% and 0.30%, respectively.

The experiments show that the shear beam bearing capacity of slender and short reinforced concrete beams decreases with increasing beam size independently of stirrups (Figs. 2.40-2.42).

Size effect tests on reinforced concrete beams were recently carried out by Belgin and Sener (2008). The beams were similar in one-, two- and three-dimensions, which means that the beam width, cover thickness, bar diameter and depth of reinforcement were all proportional to the beam span and length. In all of the specimens, the uniform bending moment was obtained between the loads. Beam lengths and widths were constant 4.6 m and 0.11 m, respectively, for the one-dimensional similarity (group I, Fig. 2.43a). Beam lengths of L=1.15 m, 2.3 m, and 4.6 m, beam widths of b=0.055 m, 0.11 m and 0.22 m, beam heights of h=0.075 m, 0.15 m, 0.30 m were used for the three-dimensional similarity (group II, Fig. 2.43b). For the two-dimensional similarities, two types of tests were carried out. For group III beam heights of h=0.15 m, 0.30 m and 0.60 m were used and a beam width was constant b=0.11 m (Fig. 2.44a). For group IV beam widths of b=0.055 m, 0.11 m and 0.22 m, beam heights of h=0.075 m, 0.15 m and 0.30 m were used and beam length was constant L=2.30 m (Fig. 2.44b). The reinforcement ratio was 3% in order to induce brittle failure.

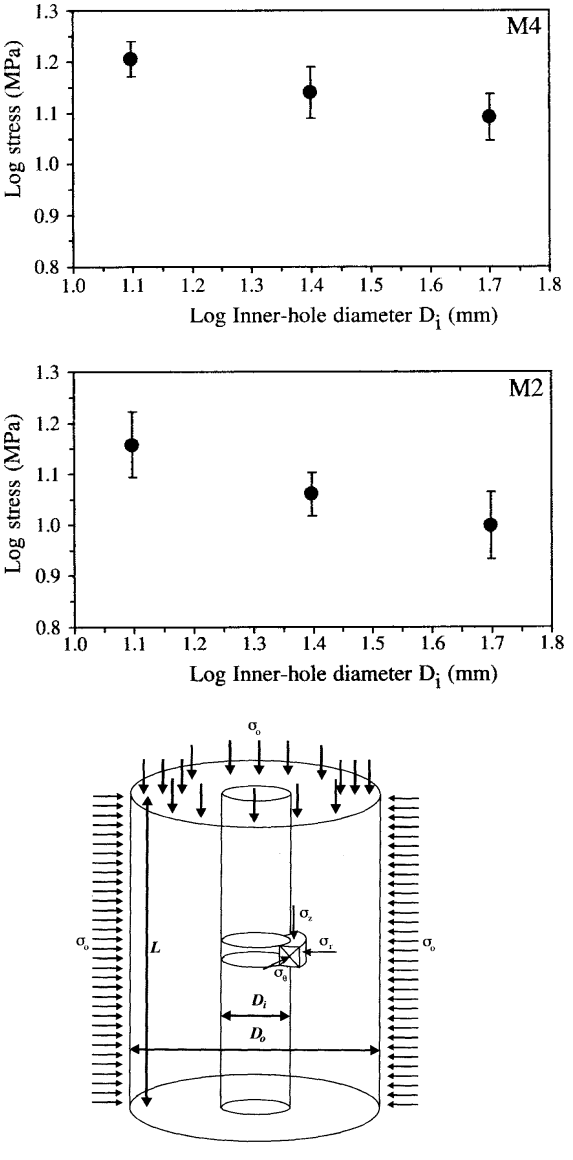

Fig. 2.29 Hollow-cylinder experiments: mean values and standard deviations for log σ versus log D_i for two different concretes (σ_o - outer stress, D_i - inner-hole diameter) (Elkadi and van Mier 2006)

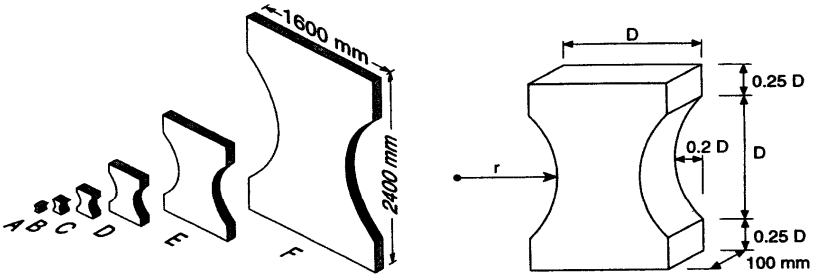

Type	A	B	C	D	E	F
D (mm)	50	100	200	400	800	1600
r (mm)	36.25	72.5	145	290	580	1160

Fig. 2.30 Specimens for size effect tests during uniaxial tension (van Vliet and van Mier 2000)

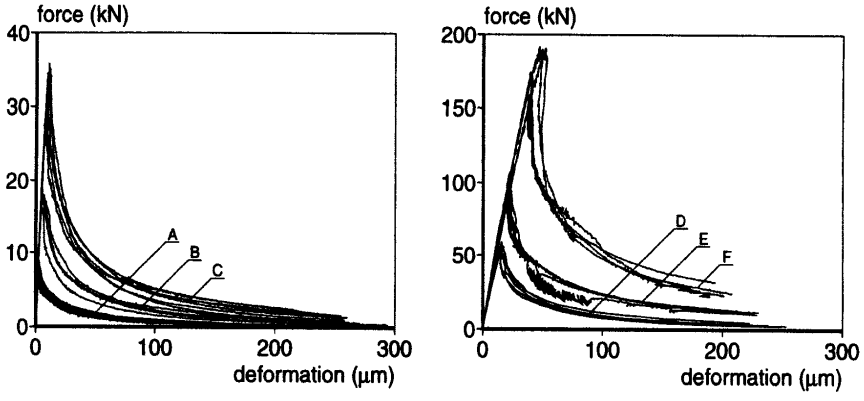

a) b)

Fig. 2.31 Experimental force-deformation curves during uniaxial tension for specimens A, B, C (a) and D, E, F (b) of Fig. 2.30 (van Vliet and van Mier 2000)

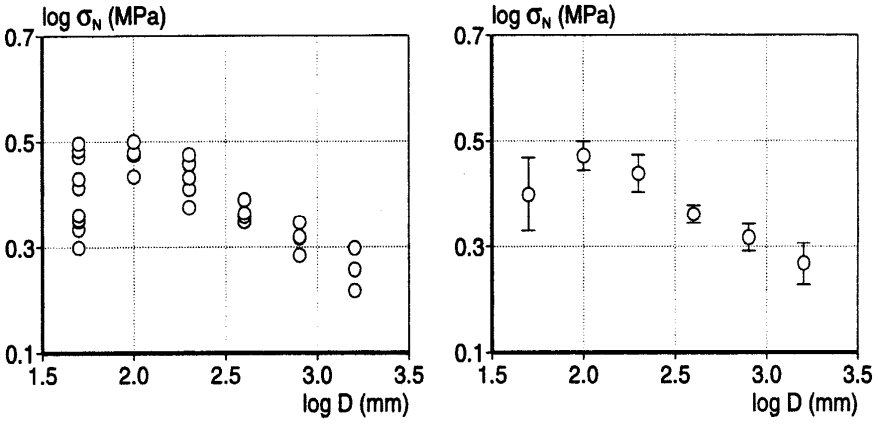

Fig. 2.32 Individual values (a) and mean values with standard deviations (b) of nominal concrete strength $\log\sigma_N$ versus specimen size D during uniaxial tension (van Vliet and van Mier 2000)

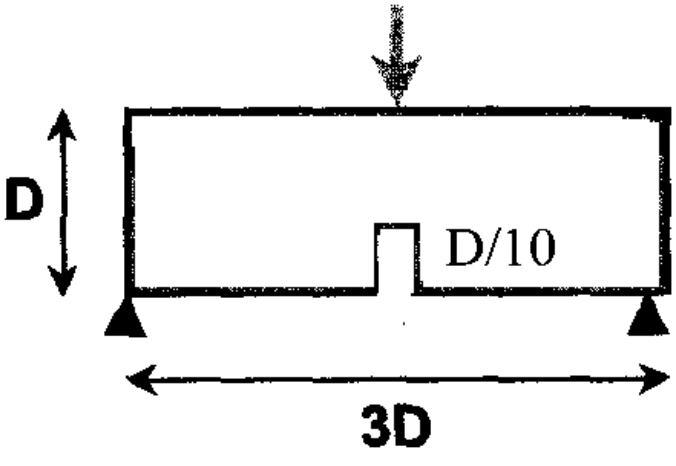

Fig. 2.33 Geometry of three-point bending size effect tests with 3 different notched beams: D_1=80 mm, D_2=160 mm, D_3=320 mm (Le Bellego et al. 2003) (D – beam height)

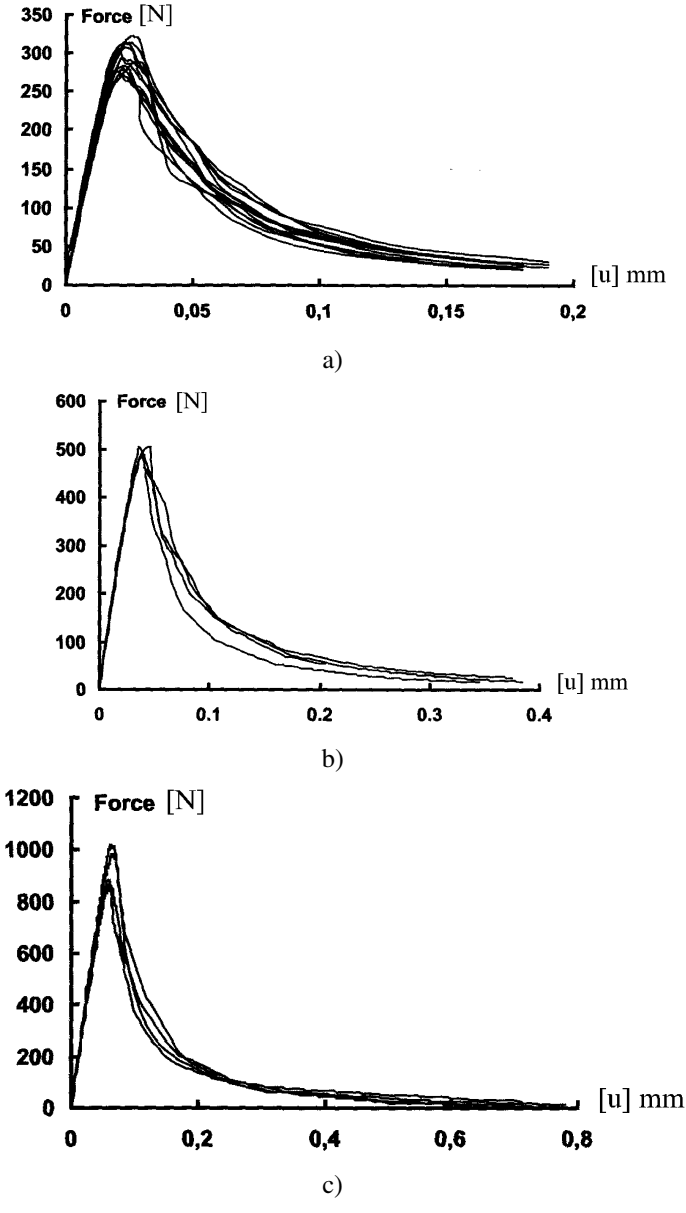

Fig. 2.34 Three point bend testing of notched beams: experimental results of vertical force versus deflection u for small- (a), medium- (b) and large-size beam (c) (Le Bellego et al. 2003)

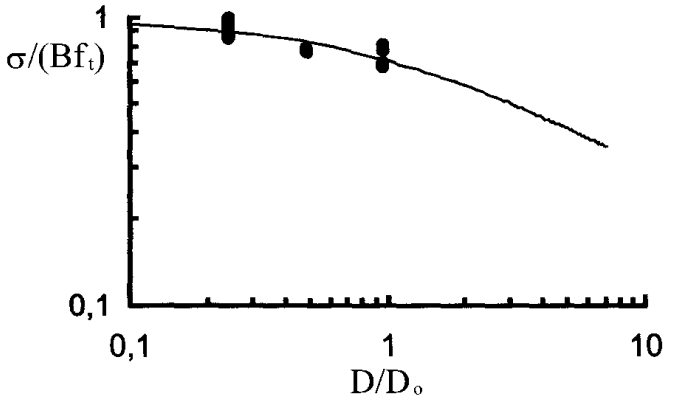

Fig. 2.35 Experimental results of size effect in three-point bending tests (points – experimental results, line – size effect law by Bažant (Bažant and Planas 1998), D – specimen size, D_o – characteristic size, B – parameter, f_t – tensile strength) (Le Bellego et al. 2003)

The beams under the constant bending moment failed by crushing of a compression zone around the peak load. Some local cracks were seen prior to crushing. The experimental results clearly confirmed the existence of a significant size effect on the nominal bending strength in beam accompanied by an increase of failure brittleness with the beam size. Figure 2.45 shows the size effect plots for the combined test results for all four groups. In the case of the two-dimensional similarity (group III and IV) tests, the maximum strengths were significantly higher than those for the one and three-dimensional similarity (group I–II) tests. For the bending tests of two-dimensional similarity (group III), the slope was e.g. 3.6 times as high as that for the three-dimensional similarity (group II) tests. Smaller beams showed a ductile behaviour compared to larger beams. The load-deflection diagrams were almost straight lines up to the peak load, after which a steeper descending branch was observed for large beams. The load-deflection diagrams for larger beams were stiffer than those for smaller beams, confirming an increase of brittleness in response to an increasing size. The post-peak behaviour was completely governed by the behaviour of concrete in a compression zone.

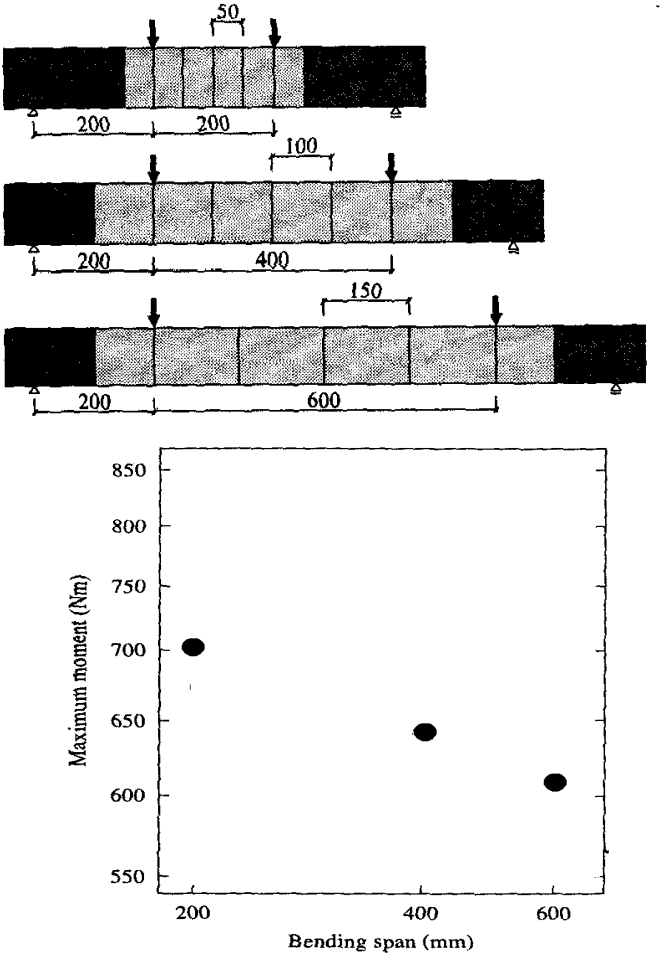

Fig. 2.36 Experimental tests with concrete beams of bending span 200 mm, 400 mm and 600 mm and measured stochastic size effect expressed by maximum bending moment against bending span (Koide et al. 1998, 2000)

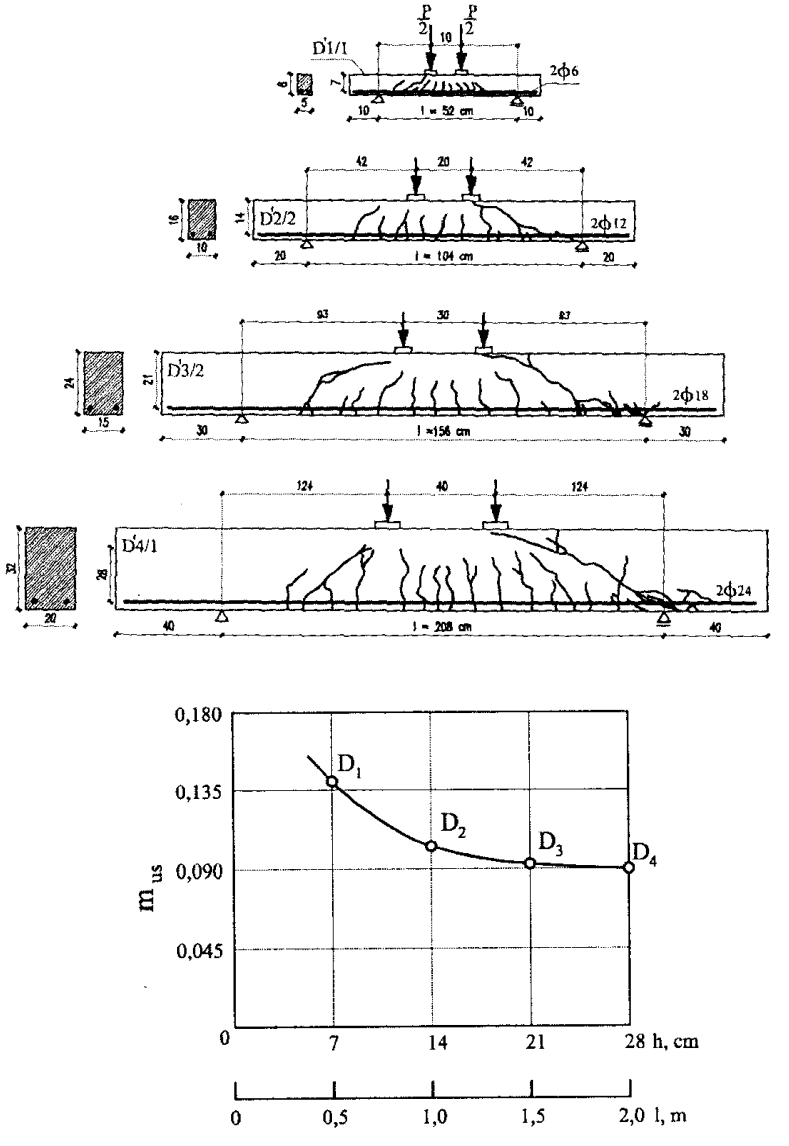

Fig. 2.37 Crack pattern and normalized failure moment against beam sizes h and l (Leonhardt and Walther 1962)

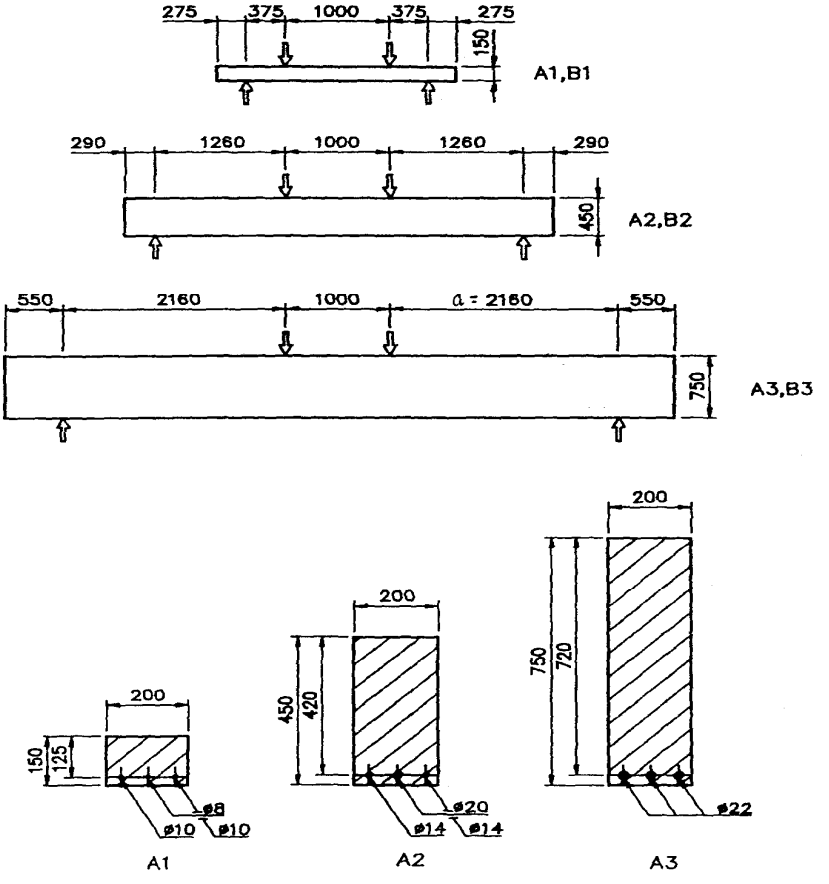

Fig. 2.38 Slender reinforced concrete beams without shear reinforcement (Walraven and Lehwalter 1994)

Bond-slip between Concrete and Reinforcement

A good bond between concrete and reinforcement is necessary for a reinforced concrete element to carry loads. A bond phenomenon was investigated by several researchers (e.g. Dörr 1980, Malvar 1992, Bolander et al. 1992, Azizinamini et al. 1993, Darwin and Graham 1993, Uijl and Bigaj 1996, Haskett et al. 2008). The experiments show that the bond stress depends on the bar roughness, bar diameter, bar location, bar ending, concrete class, bar anchorage length, direction of concrete mixing and failure mechanism (splitting or pulling out) (Idda 1999).

Fracture in concrete with a ribbed bar during a pull-out test is demonstrated in Fig. 2.46. Primary and secondary cracks occur due to the lack of bond and crushing. The effect of the bar roughness, bar location and bar ending on the

evolution of the bond stress is shown in Figs. 2.47-2.49. The bond stress increases with increasing bar roughness. It is the largest if the bar is pulled out parallel to the direction of concrete mixing (Fig. 2.48). The effect of the bar ending is also of importance (Fig. 2.49).

Figure 2.50 shows a non-linear distribution of shear stresses in the contact zone between concrete and reinforcement. With increasing pull-out force, the maximum shear stress point moves into the specimen interior.

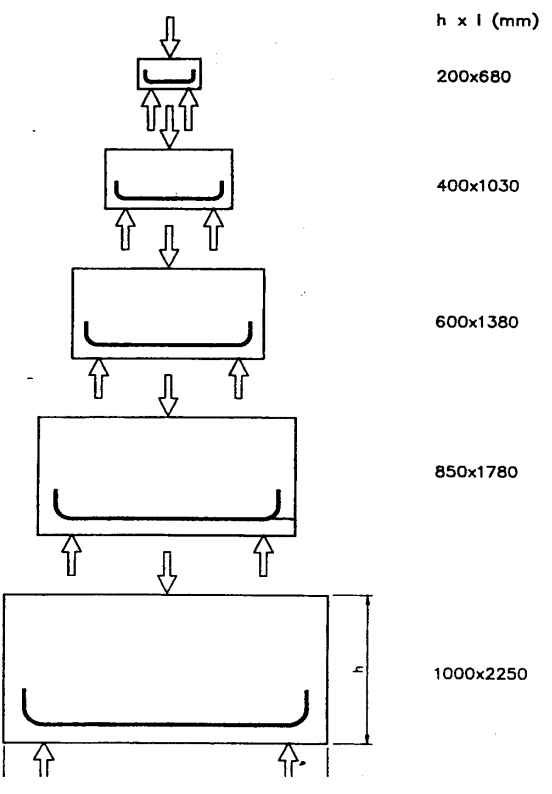

Fig. 2.39 Short reinforced concrete beams (Walraven and Lehwalter 1994)

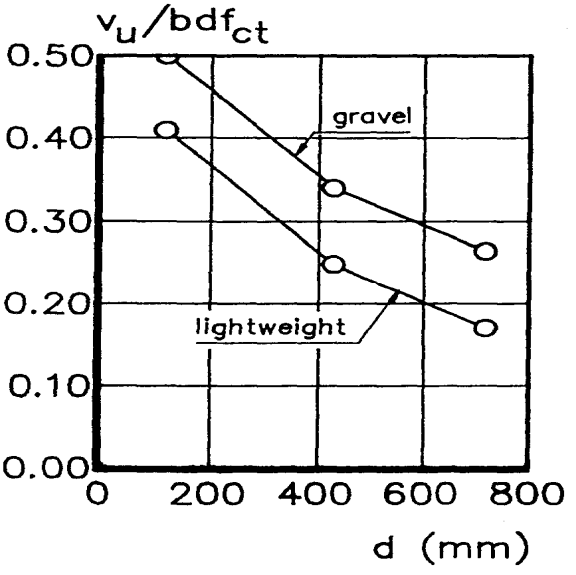

Fig. 2.40 Size effect for slender reinforced concrete beams of gravel and lightweight concrete without shear reinforcement: nominal shear strength versus effective height d (V_u - ultimate vertical force, b - beam width, f_{ct} - tensile strength) (Walraven and Lehwalter 1994)

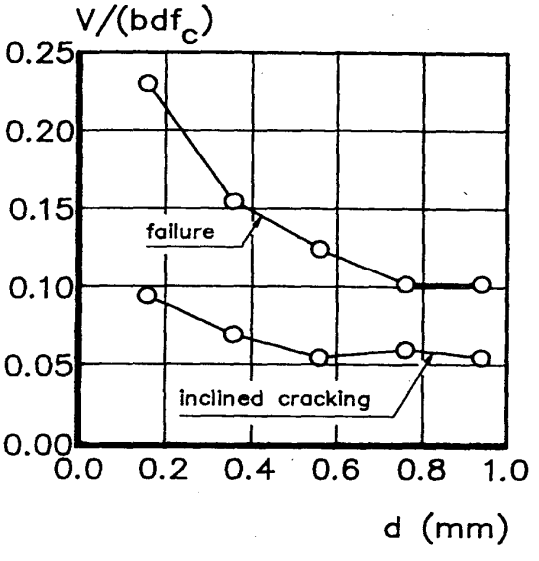

Fig. 2.41 Size effect for short reinforced concrete beams of normal concrete without shear reinforcement: nominal shear strength versus effective height d during cracking and failure (V_u - ultimate vertical force, b - beam width, f_c - compressive strength) (Walraven and Lehwalter 1994)

The bond mechanism is described in Fig. 2.51. It is accompanied by primary crack formation, bending of concrete corbels, crushing of concrete corbels connected to dilatancy and slip of separate surfaces connected to contractancy.

In turn, the experimental evolutions of the pull-out force versus slip are presented in Figs. 2.52 and 2.53. The evolution curve includes a hardening and softening phase. The pull-out force depends upon the bar diameter.

Finally, Figs. 2.54-2.57 show the effect of the reinforcement ratio, bar roughness and reinforcement cover thickness on the force-displacement curve during bending.

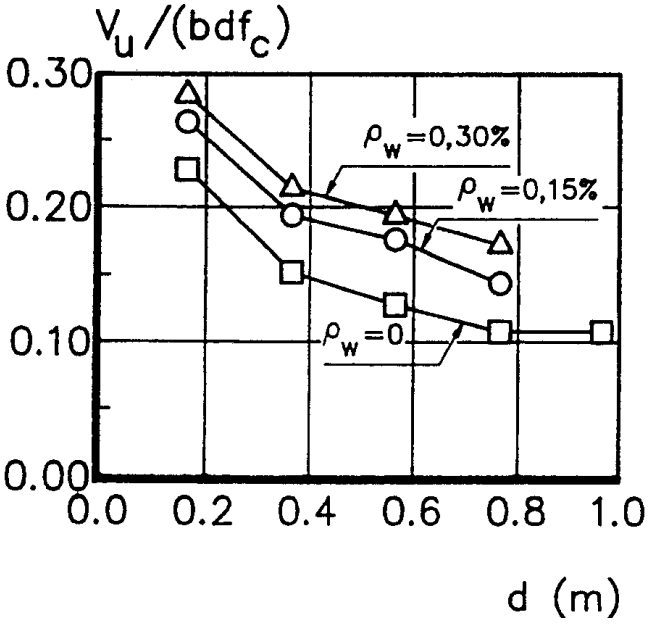

Fig. 2.42 Size effect for short reinforced concrete beams of normal concrete with shear reinforcement ratio ρ_w: nominal shear strength versus effective height d during cracking and failure (V_u - ultimate vertical force, b - beam width, f_c - compressive strength) (Walraven and Lehwalter 1994)

The results indicate that the peak and near post-peak behaviour of reinforced concrete elements are controlled by three factors: reinforcement ratio, bond-slip properties and reinforcement cover. Material softening decreases with increasing reinforcement ratio (for very low reinforcement ratios) and increases with increasing reinforcement ratio (for very high reinforcement ratios). It also decreases with increasing bar roughness. If the reinforcement cover is large enough, the specimen load exhibits a peak before the fracture zone reaches the reinforcement, then after some load decrease, the growing fracture zone reaches the reinforcement and is arrested, thus engendering hardening followed by a second peak and further softening.

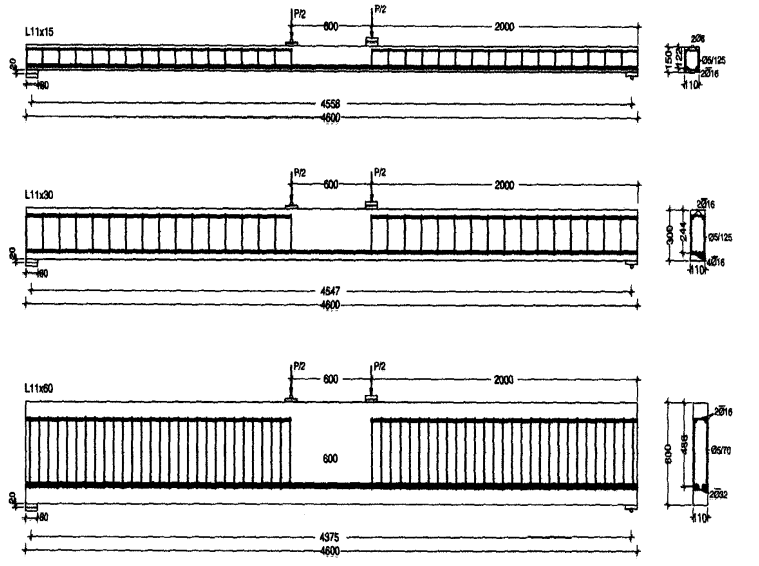

a)

b)

Fig. 2.43 Test reinforced concrete beams for group I (a) and group II (b) (Belgin and Sener 2008)

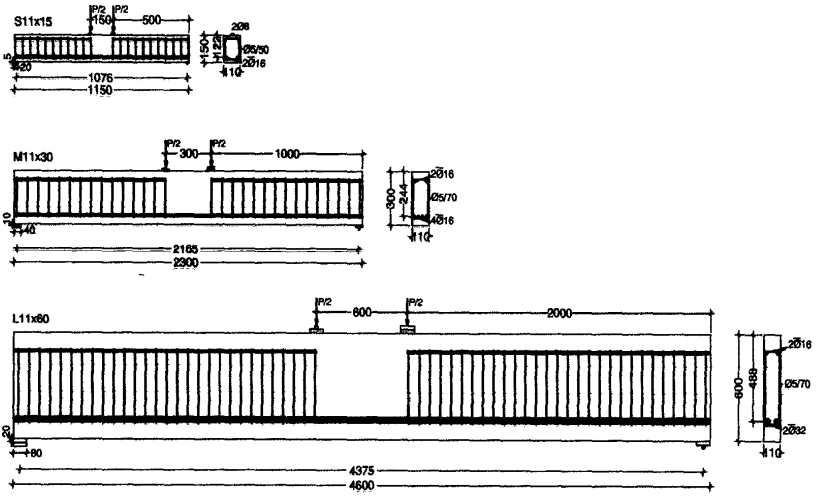

a)

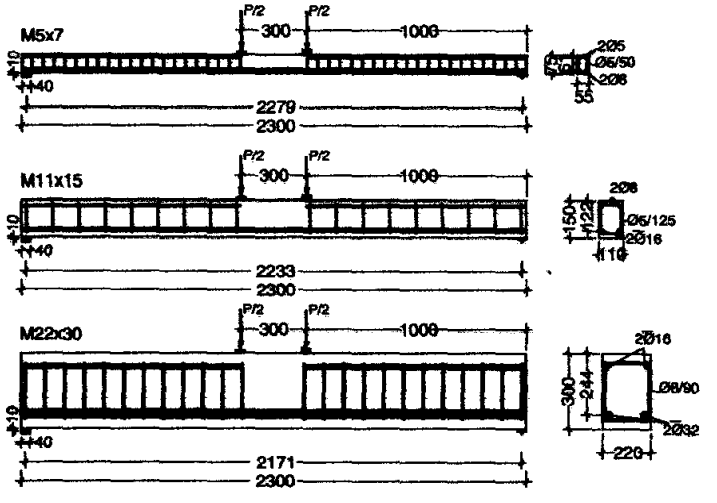

b)

Fig. 2.44 Test reinforced concrete beams for group III (a) and group IV (b) (Belgin and Sener 2008)

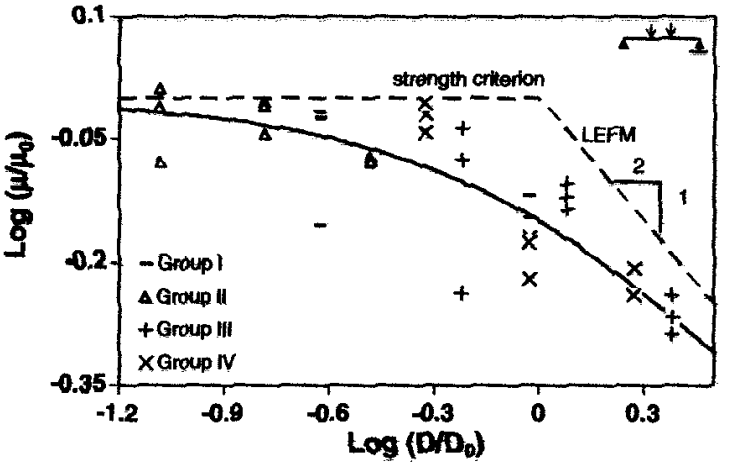

Fig. 2.45 Test results on size effect for all groups (LEFM - linear elastic fracture mechanics) (Belgin and Sener 2008)

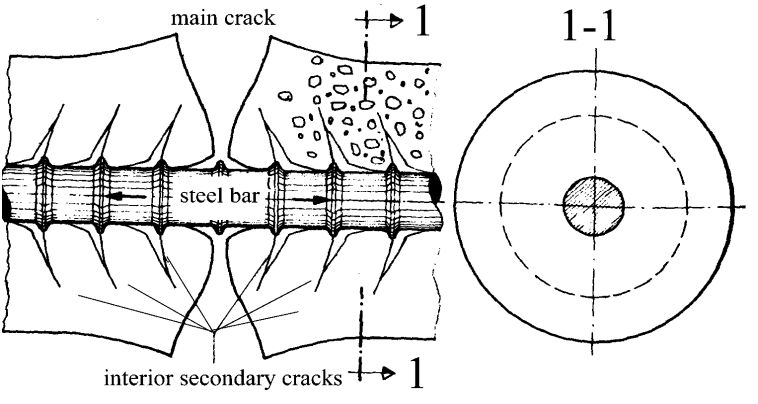

Fig. 2.46 Crack formation during pull-out test of ribbed bars (Leonhardt 1973)

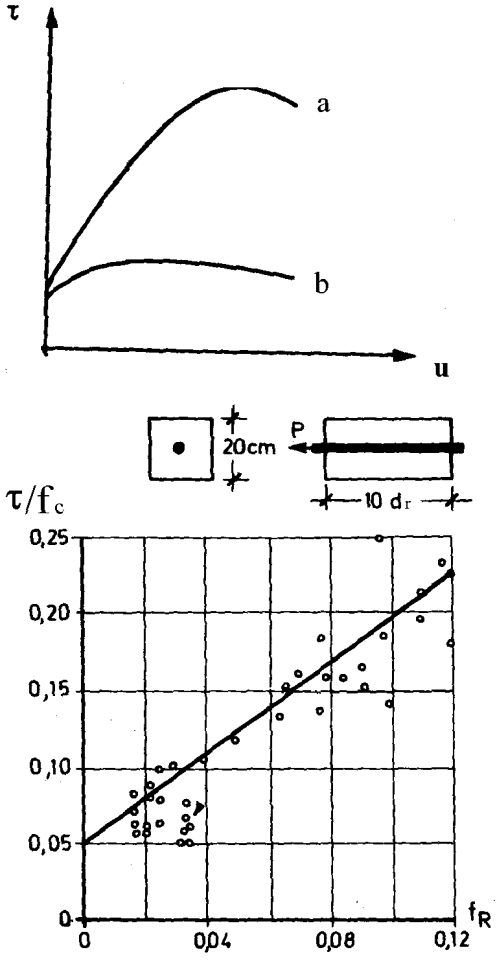

Fig. 2.47 Effect of bar roughness on evolution of bond stress τ (f_R - roughness parameter): a) very rough bars, b) smooth bars (Leonhardt 1973)

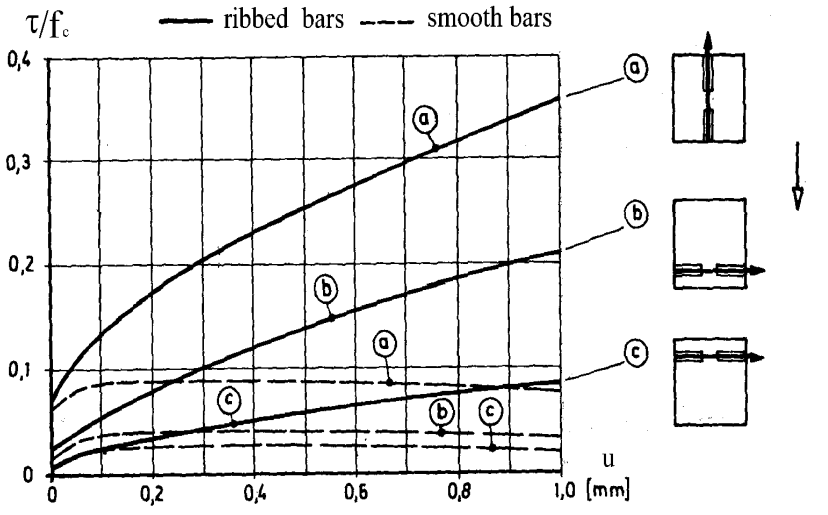

Fig. 2.48 Effect of bar location and its roughness on normalized bond stress τ/f_c (Leonhardt 1973)

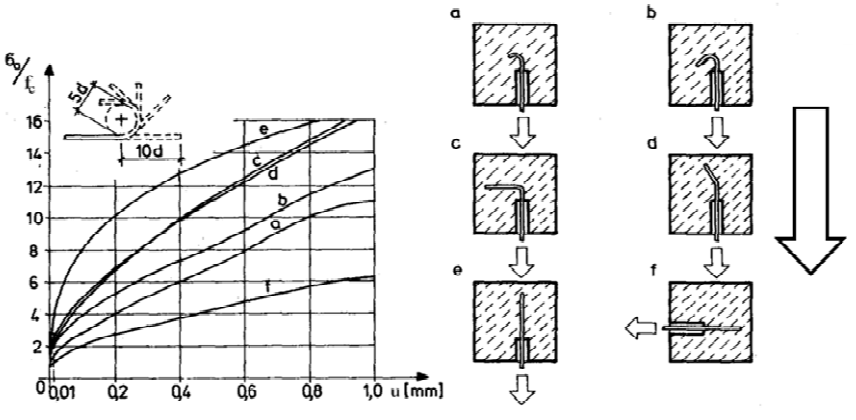

Fig. 2.49 Effect of bar ending on stresses in reinforcement (⇒ mixing direction) (Leonhardt 1973)

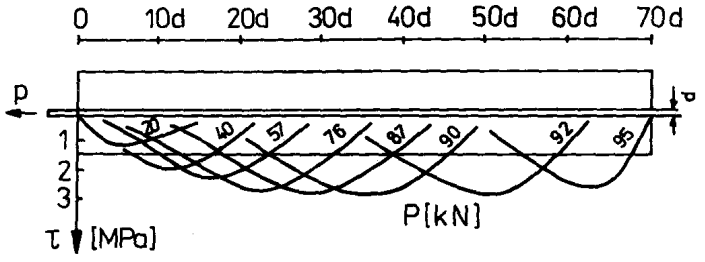

Fig. 2.50 Distribution of shear stresses τ in contact zone between concrete and reinforcement for increasing pull-out force P (Klisiński and Mróz 1988)

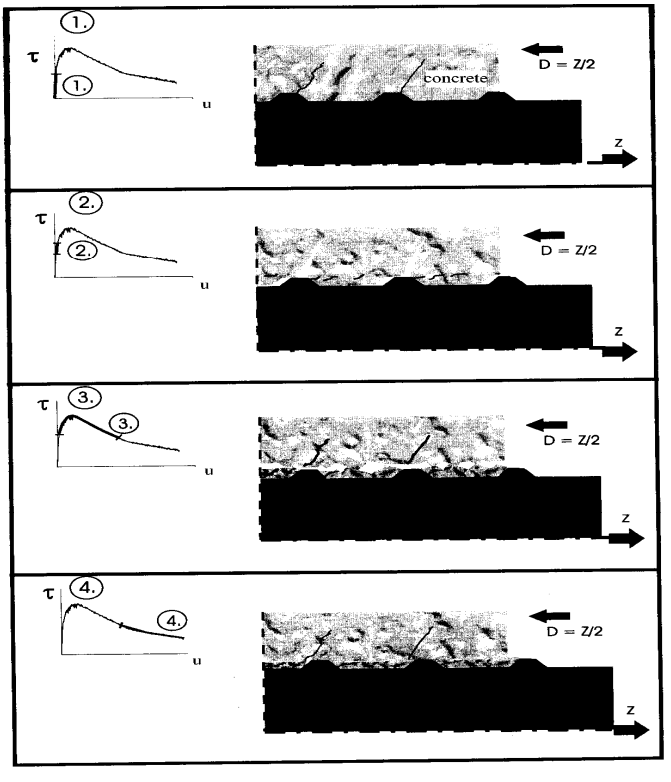

Fig. 2.51 Bond mechanism: 1. primary crack formation, 2) bending of concrete corbels, 3) crushing of concrete corbels connected to dilatancy, 4) slip of separate surfaces connected to contractancy (Idda 1999)

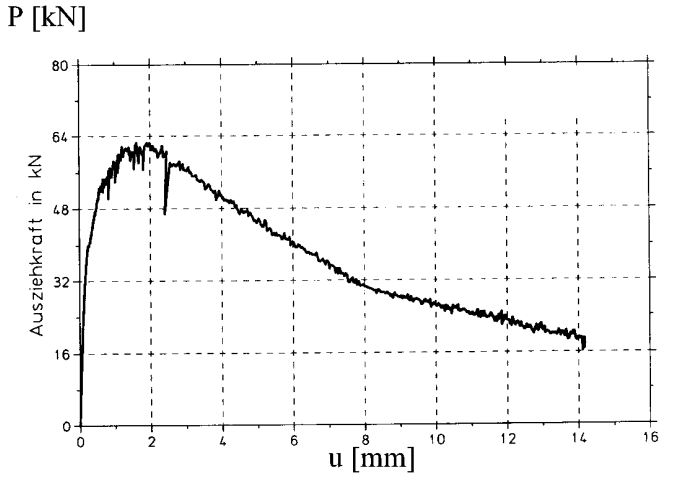

Fig. 2.52 Experimental pull-out force against slip displacement (bar diameter d_r=16 mm) (Idda 1999)

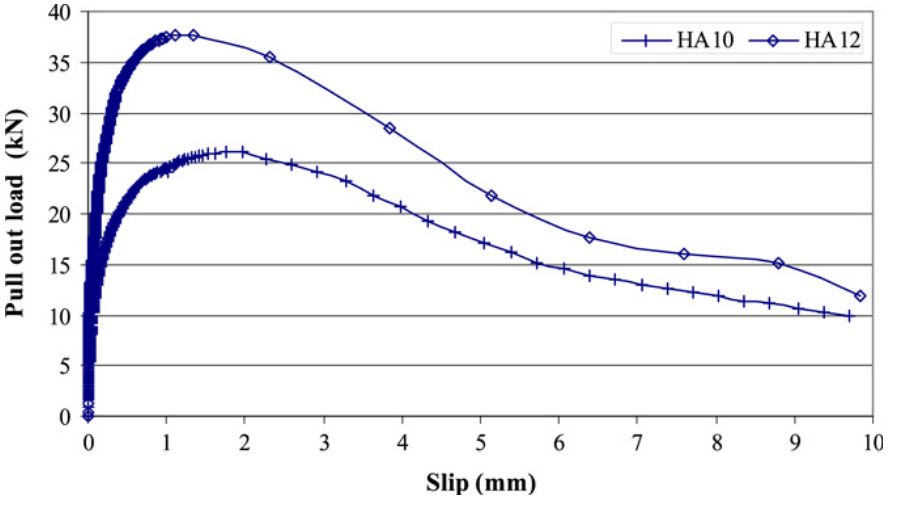

Fig. 2.53 Pull-out force versus slip for two bars with different diameter: 10 mm (HA10) and 12 mm (HA12) (Dahou et al. 2009)

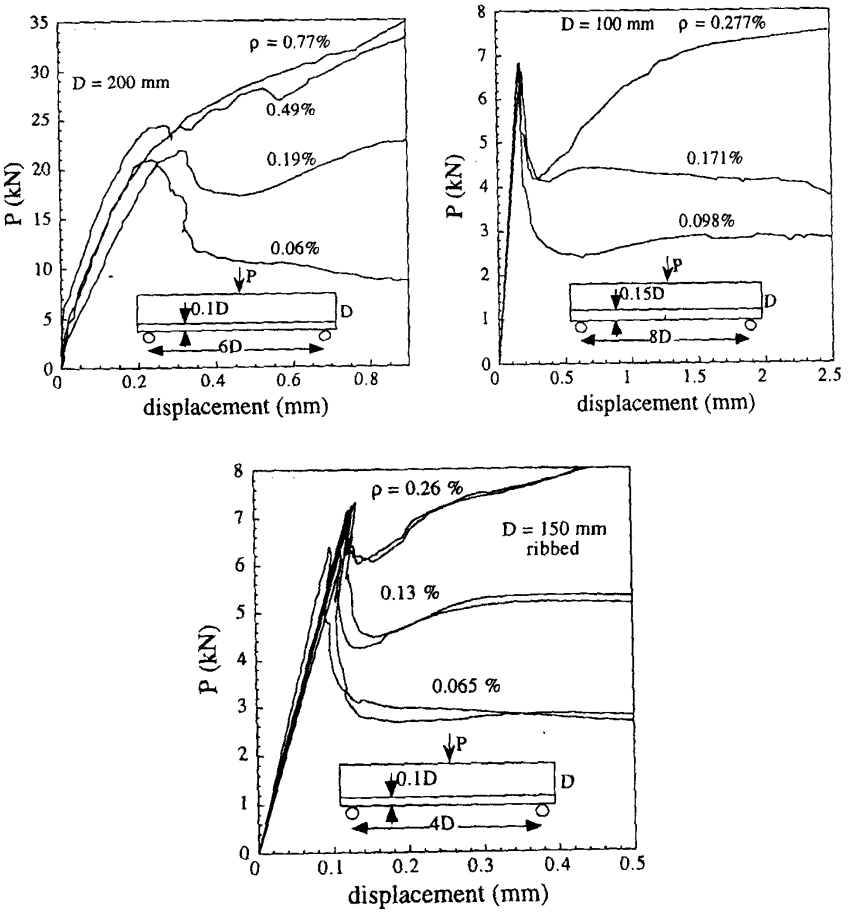

Fig. 2.54 Influence of reinforcement ratio ρ on load-deflection curve for different beam effective heights and lengths (Bažant and Planas 1998)

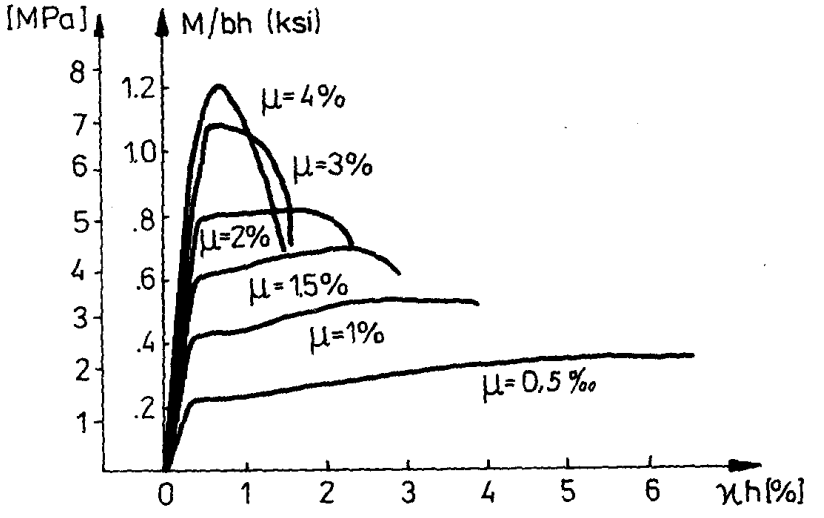

Fig. 2.55 Influence of reinforcement ratio μ on relationship between bending moment and curvature (Klisiński and Mróz 1988)

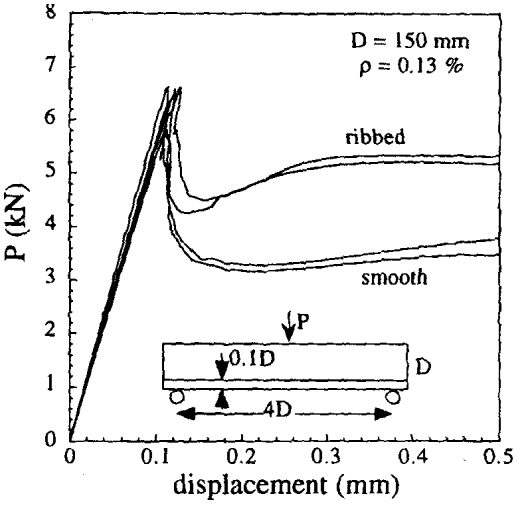

Fig. 2.56 Influence of bar roughness on load-displacement curve in reinforced concrete beams (Bažant and Planas 1998)

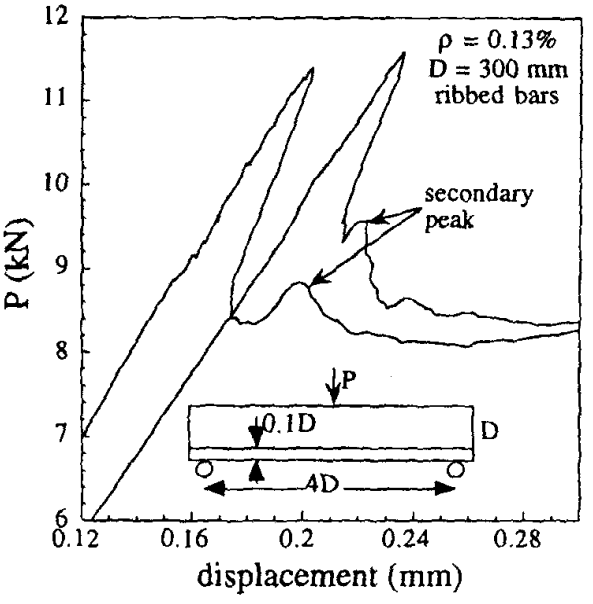

Fig. 2.57 Influence of a relatively thick cover on load-deflection curve in reinforced concrete beams (Bažant and Planas 1998)

References

Azizinamini, A., Stark, M., Roller, J.J., Ghosh, S.K.: Bond performance of reinforcing bars embedded in high-strength concrete. ACI Structural Journal (American Concrete Institute) 90(5), 554–561 (1993)

Bažant, Z., Planas, J.: Fracture and size effect in concrete and other quasi-brittle materials. CRC Press LLC (1998)

Belgin, C.M., Sener, S.: Size effect on failure of overreinforced concrete beams. Engineering Fracture Mechanics 75(8), 2308–2319 (2008)

Bischoff, P.H., Perry, S.H.: Compressive behaviour of concrete at high strain rates. Materials and Structures 24(6), 425–450 (1991)

Bischoff, P., Perry, S.H.: Impact behaviour of plane concrete loaded in uniaxial compression. Journal of Engineering Mechancis ASCE 121(6), 685–693 (1995)

Bolander, J.J., Satake, M., Hikosaka, H.: Bond degradation near developing cracks in reinforced concrete structures. Memoirs of the Faculty of Engineering 52(4), 379–395 (1992)

Dahou, Z., Mehdi, Z., Castel, A., Ghomarid, F.: Artificial neural network model for steel-concrete bond prediction. Engineering Structures 31(8), 1724–1733 (2009)

Dantu, P.: Etudes des contraintes dans les milieux heterogenes. Application au beton. Annales des l'Institut de Batiment et des Travaux Publics 11(121), 55 (1958)

Darwin, D., Graham, E.K.: Effect of deformation height and spacing on bond strength of reinforcing bars. ACI Materials Journal 90(6), 646–657 (1993)

Dörr, K.: Ein Beitag zur Berechnung von Stahlbetonscheiben unter Berücksichtigung des Verbundverhaltens. Phd Thesis, Darmstadt University (1980)

Elkadi, A.S., van Mier, J.G.M.: Experimental investigation of size effect in concrete fracture under multiaxial compression. International Journal of Fracture 140(1-4), 55–71 (2006)

Gary, G.: Essais a grande vitesse sur beton. Problemes specifiques. Scientifique Rapport GRECO edite par J.M. Reynouard, France (1990)

Godycki-Ćwirko, T.: Concrete Mechanics, Arkady (1982) (in polish)

Haskett, M., Oehlers, D.J., Mohamed Ali, M.S.: Local and global bond characteristics of steel reinforcing bars. Engineering Structures 30(2), 376–383 (2008)

Hordijk, D.A.: Local approach to fatigue of concrete, PhD Thesis, Delft University of Technology (1991)

Idda, K.: Verbundverhalten von Betonrippenstählen bei Querzug. PhD Thesis, University of Karlsruhe (1999)

Karsan, D., Jirsa, J.O.: Behaviour of concrete under compressive loadings. Journal of the Structural Division (ASCE) 95(12), 2543–2563 (1969)

Klisiński, M., Mróz, Z.: Description of inelastic deformation and damage in concrete (Opis niesprężystych deformacji i uszkodzenia betonu, in polish), Rozprawy nr.193, Poznań University of Technology, Poznań, Poland (1988)

Koide, H., Akita, H., Tomon, N.: Size effect on flexural resistance due to bending span of concrete beams. In: Mihashi, H., Rokugo, K. (eds.) Fracture Mechanics of Concrete Structures, pp. 2121–2130. Aedificatio Publishers, Freiburg (1998)

Koide, H., Akita, H., Tomon, N.: Probability model of flexural resistance on different lengths of concrete beams. In: Melchers, E., Stewart, M.G. (eds.) Application of Statistics and Probability, Balkema, vol. 2, pp. 1053–1057 (2000)

Kotsovos, M.D., Newman, J.B.: Generalized stress-strain relations for concrete. Journal of Engineering Mechanics ASCE 104(4), 845–856 (1978)

Kotsovos, M.D.: A generalized constitutive model of concrete based on fundamental material properties. Thesis, London (1980)

Kupfer, H., Hilsdorf, H.K., Rusch, H.: Behaviour of concrete under biaxial stresses. ACI Journal 65(8), 656–666 (1969)

Le Bellego, C., Dube, J.F., Pijaudier-Cabot, G., Gerard, B.: Calibration of nonlocal damage model from size effect tests. European Journal of Mechanics - A/Solids 22(1), 33–46 (2003)

Leonhardt, F., Walter, R.: Schubversuche an einfeldigen Stahlbetonbalken mit und ohne Schubbewehrung. D.A.f.Stb. 151 (1962)

Leonhardt, F.: Grundlagen zur Bemessung im Stahlbetonbau. Springer, Heidelberg (1973)

Malvar, J.: Bond of reinforcement under controlled confinement. ACI Materials Journal 189(6), 593–601 (1992)

Pivonka, P., Lackner, R., Mang, H.A.: Shapes of loading surfaces of concrete models and their influence on the peak load and failure mode in structural analyses. International Journal of Engineering Science 41(13-14), 1649–1665 (2003)

Reinhardt, H.W., Cornelissen, H.A.W., Hordijk, D.A.: Tensile tests and failure analysis of concrete. Journal of Structural Engineering ASCE 112(11), 2462–2477 (1986)

Rossi, P.: Influence of cracking in the presence of free water on the mechanical behaviour of concrete. Magazine of Concrete Research 43(154), 53–57 (1991)

Scavuzzo, R., Stankowski, T., Gerstle, K.H., Ko, H.Y.: Stress-strain curves for concrete under multiaxial load histories. Report of University of Boulder (1983)

den Uijl, J.A., Bigaj, A.: A bond model for ribbed bars based on concrete confinement. Heron 41(3), 201–226 (1996)

Walraven, J., Lehwalter, N.: Size effects in short beams loaded in shear. ACI Structural Journal 91(5), 585–593 (1994)

van Vliet, M.R.A., van Mier, J.G.M.: Softening behaviour of concrete under uniaxial compression. In: Wittmann, F.H. (ed.) Fracture Mechanics of Concrete Structures, Proc. FRAMCUS-2, pp. 383–396. Aedlflcatlo Publishers, Freiburg (1995)

van Vliet, M.R.A., van Mier, J.G.M.: Experimental investigation of concrete fracture under uniaxial compression. Mechanics of Cohesive-Frictional Materials 1(1), 115–127 (1996)

van Vliet, M.R.A., van Mier, J.G.M.: Experimental investigation of size effect in concrete and sandstone under uniaxial tension. Engineering Fracture Mechanics 65(2-3), 165–188 (2000)

Zhang, X.X., Ruiz, G., Yu, R.C., Tarifa, M.: Fracture behaviour of high-strength concrete at a wide range of loading rates. International Journal of Impact Engineering 36(10-11), 1204–1209 (2009)

Zheng, D., Li, Q.: An explanation for rate effect of concrete strength based on fracture toughness including free water viscosity. Engineering Fracture Mechanics 71(16-17), 2319–2327 (2004)